

TEON: Tensorized Orthonormalization Beyond Layer-Wise MUON for Large Language Model Pre-Training

Ruijie Zhang¹ Yequan Zhao² Ziyue Liu¹ Zhengyang Wang¹ Dongyang Li³ Yupeng Su¹ Sijia Liu⁴
Zheng Zhang²

Abstract

The MUON optimizer has demonstrated strong empirical performance in pre-training large language models by performing matrix-level gradient (or momentum)[†] orthogonalization in each layer independently. In this work, we propose **TEON**, a principled generalization of MUON that extends orthogonalization beyond individual layers by modeling the gradients of a neural network as a structured higher-order tensor. We present TEON’s improved convergence guarantee over layer-wise MUON, and further develop a practical instantiation of TEON based on the theoretical analysis with corresponding ablation. We evaluate our approach on two widely adopted architectures: GPT-style models, ranging from 130M to 774M parameters, and LLaMA-style models, ranging from 60M to 1B parameters. Experimental results show that TEON consistently improves training and validation perplexity across model scales and exhibits strong robustness under various approximate SVD schemes.

1. Introduction

Following the scaling laws (Kaplan et al., 2020; Hoffmann et al., 2022; Kumar et al., 2025), models like GPT, DeepSeek, LLaMA and Gemini (Achiam et al., 2023; Liu et al., 2024a; Grattafiori et al., 2024; Team et al., 2023) have made remarkable advances in artificial general intelligence. However, as both model size and training data volume continue to grow to an extreme scale, pre-training large foundation models has become super resource-intensive. This trend has motivated renewed interest in improving pre-training

¹Computer Science, UC Santa Barbara ²Electrical & Computer Engineering, UC Santa Barbara ³Mathematics, UC Santa Barbara

⁴Computer Science & Engineering, Michigan State University. Correspondence to: Zheng Zhang <zhengzhang@ece.ucsb.edu>.

Preprint. February 2, 2026.

[†] For simplicity, we use gradient orthogonalization in the following discussion.

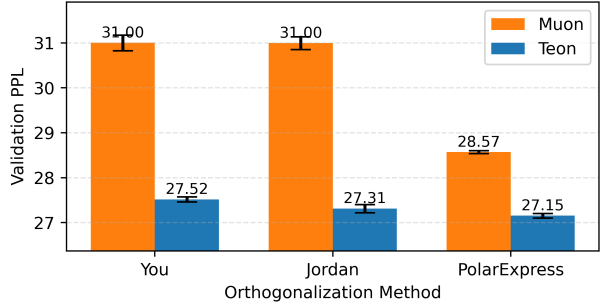


Figure 1. Pre-training GPT-Small on 10 Billion FineWeb Tokens. We run 5 trials with different random seeds to estimate the standard deviations. Validation perplexity (PPL) is reported; lower is better. Our proposed method TEON, consistently outperforms MUON across different orthogonalization methods. Additional experimental results across various model configurations are presented, with more detailed analysis in Section 5.

efficiency (Mehmood et al., 2023; Han et al., 2024; You et al., 2019; Zhao et al., 2024; Zhang et al., 2025; Liu et al., 2025b). In this context, optimizers play a pivotal role in enabling efficient training. Over the years, substantial progress has been made (Kingma, 2014; Loshchilov & Hutter, 2017; Liu et al., 2024b; Jordan et al., 2024; Yuan et al., 2024; Vyas et al., 2025; Li, 2018a;b; Pooladzandi & Li, 2024; Li, 2022; 2024; Pethick et al., 2025) in developing efficient optimizers for large-scale training. Among them, Adam (Kingma, 2014) and its variant AdamW (Loshchilov & Hutter, 2017) have become the most widely used optimizers.

Recently, the MUON optimizer, proposed by (Jordan et al., 2024), has attracted increasing attention in the pre-training community. MUON updates the model parameters by orthogonalizing the gradient momentum using Newton–Schulz iterations, effectively mitigating the collapse of the gradient rank. Initial studies demonstrate that MUON achieves promising results in small-scale LLM training, and subsequent works (Liu et al., 2025a) further show that it can be scaled to the pre-training of large foundation models. Following this observation, many large foundation models (Team et al., 2025a; Ding et al., 2025; Zeng et al., 2025; Team et al., 2025b) have adopted the Muon optimizer during pre-training and have achieved improved overall perfor-

mance. Many other works also explore the efficiency, effectiveness, scalability, and interpretability of MUON (Bernstein, 2025; Khaled et al., 2025; Amsel et al., 2025; Li et al., 2025; Kovalev, 2025).

Despite these successes, existing MUON-based approaches operate in a layer-wise manner, treating each layer independently and thereby neglecting correlations across layers. Motivated by this limitation, we propose **TEON**, a **T**ensor-level generalization of **MUON** that extends gradient orthogonalization beyond individual layers. Rather than performing gradient orthogonalization on a per-layer basis, TEON jointly considers multiple layers and applies gradient orthogonalization on a higher-order tensor, enabling the optimizer to capture cross-layer correlations during training. We also develop a practical variant of TEON. As shown in Figure 1, TEON consistently outperforms MUON.

We summarize our contributions as follows:

- We propose **TEON**, a generalization of the MUON optimizer that extends gradient orthogonalization from individual matrices to structured tensors.
- We develop a theoretical analysis showing that TEON offers stronger convergence guarantees than MUON, providing algorithmic insights into practical design guidance. These guidelines are validated through extensive ablation studies to yield the best practical TEON for LLMs pre-training.
- We conduct pre-training experiments comparing TEON and MUON across GPT-style and LLaMA-style models at various scales, under diverse training configurations, to demonstrate the effectiveness and robustness of TEON.

2. Preliminary

2.1. Layer-wise MUON

Unlike Adam/SGD-based optimizers, MUON (Jordan et al., 2024) operates on a matrix rather than a vector. By enforcing orthogonalization on the layer-wise gradient, MUON prevents the rank collapse of the gradient by replacing the singular value matrix with an identity matrix. Let η and μ denote the learning rate and the momentum coefficient, respectively. Assume that $\mathbf{W}_t \in \mathbb{R}^{m \times n}$ is the layer being adapted at iteration t , $\mathbf{G}_t \in \mathbb{R}^{m \times n}$ is its stochastic gradient, and \mathbf{M}_t is the gradient momentum at iteration t . The MUON update is given by

$$\begin{aligned} \mathbf{M}_t &= \mu \mathbf{M}_{t-1} + (1 - \mu) \mathbf{G}_t \\ \mathbf{O}_t &= \text{Ortho}(\mathbf{M}_t) \\ \mathbf{W}_t &= \mathbf{W}_{t-1} - \eta \cdot \sqrt{m/n} \cdot \mathbf{O}_t \end{aligned} \quad (1)$$

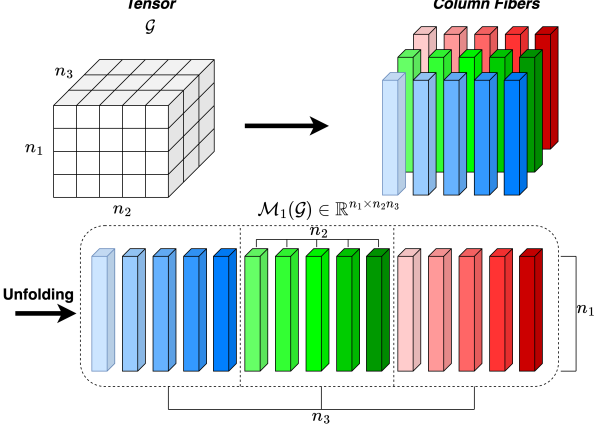


Figure 2. Mode-1 Matricization of a given tensor \mathcal{G} . \mathcal{G} is first sliced into its column fibers, i.e., vectors obtained by fixing all indices except the first, and these fibers are then arranged as columns of a matrix to form the mode-1 unfolding.

where $\text{Ortho}(\cdot)$ denotes the semi-orthogonal matrix function closest to the input matrix (Higham, 2008). Specifically, if the SVD of the input matrix \mathbf{M} is $\mathbf{M} = \mathbf{U}\Sigma\mathbf{V}^T$, then $\text{Ortho}(\mathbf{M}) := \mathbf{U}\mathbf{V}^T$. In practice, the Newton-Schulz iteration process (Higham, 2008) is commonly used to approximate the SVD. The dimensional pre-factor $\sqrt{m/n}$ was suggested by (Bernstein, 2025) for better scalability. In addition, various other methods have been explored to improve the accuracy and speed of this approximation (Amsel et al., 2025; Cesista et al., 2025).

2.2. Tensor: notations and definitions

A tensor is a multidimensional array that generalizes vectors and matrices to higher orders (Kolda & Bader, 2009). The *order* of a tensor refers to the number of its dimensions (or modes). Let $\mathcal{G} \in \mathbb{R}^{n_1 \times n_2 \times \dots \times n_d}$ denote an order- d tensor, where n_i is the size of the i -th mode. Let $g_{i_1 i_2 \dots i_d}$ denote the (i_1, i_2, \dots, i_d) -th element of \mathcal{G} , then for two tensors \mathcal{G} and \mathcal{W} with the same size, their inner product is defined as

$$\langle \mathcal{G}, \mathcal{W} \rangle = \sum_{i_1=1}^{n_1} \dots \sum_{i_d=1}^{n_d} g_{i_1 i_2 \dots i_d} w_{i_1 i_2 \dots i_d}. \quad (2)$$

The Frobenius norm of a tensor \mathcal{G} is defined as

$$\|\mathcal{G}\|_F = \sqrt{\langle \mathcal{G}, \mathcal{G} \rangle}. \quad (3)$$

Matricization and folding. A tensor can be unfolded along a selected mode to form a matrix, which is called matricization. The *mode- i matricization* of \mathcal{G} , denoted by $\mathcal{M}_i(\mathcal{G})$, reshapes the tensor into a matrix by unfolding \mathcal{G} along its i -th mode. As shown in Figure 2, the fibers of \mathcal{G} along the i -th dimension are vectorized and stacked as the rows of the resulting matrix. As a result, the mode- i matricization has the shape

$$\mathcal{M}_i(\mathcal{G}) \in \mathbb{R}^{n_i \times (\prod_{j \neq i} n_j)}.$$

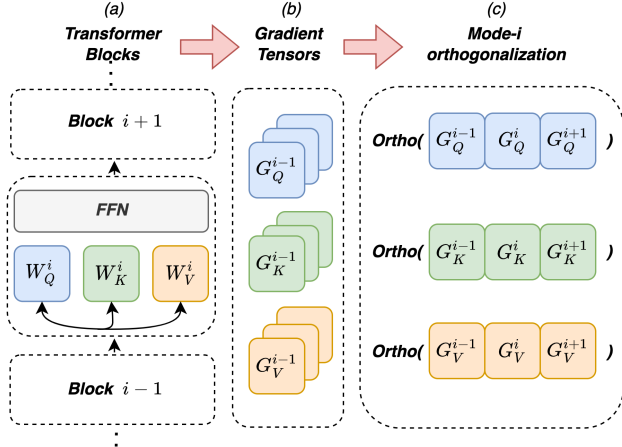


Figure 3. Overview of TEON. (a) **Transformer blocks**: Gradients are collected from K successive layers ($K = 3$ in this figure). (b) **Gradient tensors**: Gradients of the same layer type are stacked to form structured gradient tensors. (c) **Mode- i orthogonalization**: The gradient tensor is matricized along mode i , followed by MUON-style orthogonalization on the resulting matrix, which is then used to update the parameters accordingly.

We use \mathcal{M}_i^{-1} to denote the inverse operator, which converts the mode- i matricized result back to the original tensor.

3. The TEON Method

We are inspired by the Fisher information matrix underlying natural gradient methods (Amari, 1998). In principle, the optimal natural gradient is defined with respect to the Fisher metric of the *entire vectorized model parameters*, resulting in a dense and intractable matrix. Consequently, practical optimizers rely on various approximations. For instance, Adam can be interpreted as using a diagonal approximation of the Fisher matrix, which ignores inter-parameter correlations (Hwang, 2024). MUON operates on layer-wise matrices rather than individual parameter vectors; however, it does not model inter-layer correlations, which is formally analogous to diagonal approximations used in Adam. Therefore, we ask the following question:

Can we extend MUON to account for the correlations across multiple matrices?

3.1. From Layer-wise to Tensor-wise Modeling: The TEON Optimizer

We now introduce TEON, a generalization of the MUON optimizer that extends layer-wise gradient orthogonalization to a tensor-based formulation, which attempts to capture correlations among gradients from multiple layers. A natural approach is to stack a set of layer gradients together into a single tensor and use *tensor orthogonalization* to constrain the update direction. Specifically, TEON first stack gradients across multiple identical layers $\mathbf{G}^{(1)}, \dots, \mathbf{G}^{(K)}, \mathbf{G}^{(k)} \in \mathbb{R}^{m \times n}$ into an order-3 tensor:

$$\text{Ten}(\mathbf{G}^1, \dots, \mathbf{G}^K) = \mathcal{G} \in \mathbb{R}^{m \times n \times K}, \mathcal{G}[:, :, \ell] = \mathbf{G}^{(k)} \quad (4)$$

and then orthogonalize the gradient tensor \mathcal{G} .

However, unlike matrix orthogonalization, there is no unique or universally accepted notion of tensor orthogonalization. Existing approaches typically rely on reducing the tensor to a matrix representation before applying matrix-based orthogonalization procedures. In this work, we adopt a strategy known as *matricization-based tensor orthogonalization*, where a tensor is first unfolded along a selected mode (e.g. Figure 2) and then orthogonalized through the corresponding matrix representation. Specifically, for $i \in \{1, 2, 3\}$, let $\mathcal{M}_i(\mathcal{G})$ denote the mode- i matricization. Then we have

$$\begin{aligned} \mathcal{M}_1(\mathcal{G}) &\in \mathbb{R}^{m \times (nK)}, & \mathcal{M}_2(\mathcal{G}) &\in \mathbb{R}^{n \times (mK)}, \\ \mathcal{M}_3(\mathcal{G}) &\in \mathbb{R}^{K \times (mn)}. \end{aligned} \quad (5)$$

The mode- i orthogonalization of tensor \mathcal{G} is defined as

$$\mathcal{O}_i(\mathcal{G}) := \mathcal{M}_i^{-1}(\text{Ortho}(\mathcal{M}_i(\mathcal{G}))). \quad (6)$$

where $\text{Ortho}(\cdot)$ is the same orthogonalization operator used in Section 2.1. Finally, as shown in Figure 3, the update step at time t of TEON is summarized as:

$$\begin{aligned} \mathcal{T}_t^l &= \text{Ten}(\mathbf{M}_t^a, \dots, \mathbf{M}_t^b) \\ \mathcal{O}_t^l &= \mathcal{M}_i^{-1}(\text{Ortho}(\mathcal{M}_i(\mathcal{T}_t^l))) \\ \mathcal{W}_t^l &= \mathcal{W}_{t-1}^l - \eta \cdot \sqrt{m/n} \cdot \mathcal{O}_t^l \end{aligned} \quad (7)$$

Here, \mathbf{M}_t^k represents the momentum matrix from the k -th layer, and \mathcal{T}_t^l is the stacked momentum tensor formed by combining momentum matrices from the a -th to the b -th layer, where $l = b - a + 1$. Similarly, $\mathcal{W}_t^l = \text{Ten}(\mathbf{W}_t^a, \dots, \mathbf{W}_t^b)$ denotes the stacked weight tensor over the same layer range.

3.2. Implementation of TEON

The implementation of TEON involves the choice of some hyper-parameters. Specifically:

- **Matricization mode i** : since mode 3 has an extremely unbalanced and large size, we choose to matricize mode 1 or 2. In practice, we choose $i = 1$ to achieve the best performance based on the theoretical analysis in Section 4.1 and the ablation study in Section 6.1.
- **Number of stacking layers K** : the choice of K depends on the trade-off between the potentially optimal performance gain and the actual correlation among stacked layers. We choose $K = 2$ based on the theoretical analysis in Section 4.1 and the ablation study in Section 6.3.

Algorithm 1 TEON (mode-1 orthogonalization)

Require: Parameters $\{\mathbf{X}_t^{(k)}\}_{n=1}^N$, steps T , learning rate η , momentum μ , group size K .

Ensure: Updated parameters $\{\mathbf{X}_t^{(k)}\}_{n=1}^N$

- 1: **for** $t \leftarrow 0$ **to** $T - 1$ **do**
- 2: Compute gradient $\{\mathbf{G}_t^{(k)}\}_{n=1}^N$ for $\{\mathbf{X}_t^{(k)}\}_{n=1}^N$
- 3: **for** $i \leftarrow 0$ **to** $\lfloor N/K \rfloor$ **do**
- 4: Form tensor $\mathbf{g}_t \in \mathbb{R}^{m \times n \times K}$ with $\mathbf{g}_t[:, :, k] = \mathbf{G}_t^{(iK+k)}$
- 5: $\mathcal{M}_t \leftarrow \mu \mathcal{M}_{t-1} + \mathbf{g}_t$
- 6: $\mathbf{Z}_t \leftarrow \mathcal{M}_1(\mathcal{M}_t)$
- 7: $\mathbf{Q}_t \leftarrow \text{Ortho}(\mathbf{Z}_t)$
- 8: $\mathbf{U}_t \leftarrow \mathcal{M}_1^{-1}(\mathbf{Q}_t)$
- 9: **for** $k \leftarrow 1$ **to** K **do**
- 10: $\mathbf{X}_{t+1}^{(iK+k)} \leftarrow \mathbf{X}_t^{(iK+k)} - \eta \sqrt{m/n} \mathbf{U}_t[:, :, k]$
- 11: **end for**
- 12: **end for**
- 13: **end for**

- **The layers selected for stacking:** for transformer architecture, we stack the gradient matrices of \mathbf{Q} , \mathbf{K} and \mathbf{V} from two consecutive layers. This is because they have the strongest correlated top singular vectors, which is supported by the theory in Section 4.1 and the ablation study in Section 6.2.

In the next section, we will explain the theoretical benefit of TEON and justify the above implementation choices.

4. Theoretical Analysis of TEON

In this section, we provide some key theoretical analysis to answer the following key questions:

- Why can TEON offer stronger convergence guarantees than MUON?
- Why should we choose the algorithm design parameters as in Section 3.2?

We first provide the key results and their practical implications in Section 4.1, then provide a sketch of proof in Section 4.2.

4.1. Main Theoretical Results

4.1.1. DEFINITIONS AND ASSUMPTIONS

We study TEON and MUON based on the Non-Euclidean Trust Region (NTR) formulation (Kovalev, 2025), a template for steepest-descent in Non-Euclidean norms. We extend the analysis when the objective $\mathbf{W} \in \mathbb{R}^{m \times n \times K}$ is a tensor of stacked parameters.

We first define MUON and TEON norms as follows.

Definition 4.1 (MUON and TEON norms). Let $\mathbf{X} \in \mathbb{R}^{m \times n \times K}$ with slices $\mathbf{X}[:, :, k] = \mathbf{X}^{(k)} \in \mathbb{R}^{m \times n}$. For

$i \in \{1, 2, 3\}$, let $\mathcal{M}_i(\mathbf{X})$ denote the mode- i matricization. We define a TEON family of norms parameterized by the mode- i matricization:

$$\|\mathbf{X}\|_{\text{TEON}-i} := \|\mathcal{M}_i(\mathbf{X})\|_{\text{op}}, \|\mathbf{X}\|_{\text{TEON}-i,*} := \|\mathcal{M}_i(\mathbf{X})\|_*$$

We also define the MUON norm and its dual:

$$\|\mathbf{X}\|_{\text{MUON}} := \max_{k \in [K]} \|\mathbf{X}^{(k)}\|_{\text{op}}, \|\mathbf{X}\|_{\text{MUON},*} := \sum_{k=1}^K \|\mathbf{X}^{(k)}\|_*$$

Detailed derivations are provided in Appendix A.1.

We adopt standard assumptions under the NTR framework following (Kovalev, 2025; Khaled et al., 2025).

Assumption 4.2 (Smoothness). Let $\|\cdot\|$ be a norm on $\mathbb{R}^{m \times n \times L}$ with dual $\|\cdot\|_*$. The objective f is L -smooth w.r.t. $\|\cdot\|$ if for all \mathbf{W}, \mathbf{W}' ,

$$\|\nabla f(\mathbf{W}) - \nabla f(\mathbf{W}')\|_* \leq L \|\mathbf{W} - \mathbf{W}'\|. \quad (8)$$

Assumption 4.3 (Unbiased gradients and bounded variance). Stochastic gradients $\mathbf{G}(\mathbf{W}; \xi)$ satisfy $\mathbb{E}_\xi[\mathbf{G}(\mathbf{W}; \xi)] = \nabla f(\mathbf{W})$ and $\mathbb{E}_\xi[\|\mathbf{G}(\mathbf{W}; \xi) - \nabla f(\mathbf{W})\|_F^2] \leq \sigma^2$.

Assumption 4.4 (Norm–Frobenius equivalence). There exists $\rho > 0$ such that $\|\mathbf{X}\| \leq \rho \|\mathbf{X}\|_F$.

With a chosen norm and its dual norm $(\|\cdot\|, \|\cdot\|_*)$, each NTR step with momentum can be written as follows:

$$\begin{aligned} \mathcal{M}_t &= \mu \mathcal{M}_{t-1} + \mathbf{g}_t, \\ \mathbf{W}_{t+1} &= \underset{\|\mathbf{W} - \mathbf{W}_t\| \leq \eta}{\operatorname{argmin}} \langle \mathcal{M}_t, \mathbf{W} - \mathbf{W}_t \rangle, \end{aligned} \quad (9)$$

where \mathbf{g}_t is a stochastic gradient, $\mu \in [0, 1]$ and $\eta > 0$. The NTR step with the norms defined in Definition A.2 recovers the corresponding TEON and MUON updates in Appendix A.2.

4.1.2. KEY RESULTS.

The first theorem shows that TEON can achieve the same or up to $\sqrt{K} \times$ better convergence bound than MUON.

Theorem 4.5 (Convergence Bound). Consider minimizing $f(\mathbf{W})$, $\mathbf{W} \in \mathbb{R}^{m \times n \times K}$ and suppose f is lower bounded by f^* . Define the best iterates of MUON and TEON as $\tau_{\text{MUON}} := \arg \min_{0 \leq t < T} \|\nabla f(\mathbf{W}_t)\|_{\text{MUON},*}$ and $\tau_{\text{TEON}} := \arg \min_{0 \leq t < T} \|\nabla f(\mathbf{W}_t)\|_{\text{TEON},*}$.

Under the same TEON norm (c.f. Definition 4.1), the convergence bounds satisfy:

$$\begin{aligned} \|\nabla f(\mathbf{W}_{\tau_{\text{TEON}}})\|_{\text{TEON},*} &\leq \sqrt{\frac{2L_{\text{TEON}}(f(\mathbf{W}_0) - f^*)}{T}}, \\ \|\nabla f(\mathbf{W}_{\tau_{\text{MUON}}})\|_{\text{TEON},*} &\leq \sqrt{\frac{2L_{\text{MUON}}(f(\mathbf{W}_0) - f^*)}{T}}. \end{aligned}$$

The smoothness constants satisfy $L_{\text{TEON}} \leq L_{\text{MUON}} \leq K L_{\text{TEON}}$.

When the smoothness constant $L_{\text{TEON}} \approx L_{\text{MUON}}$, the convergence guarantees of THE TEON and MUON match up to constants. In the best case, TEON has an improved convergence bound over MUON by $\sqrt{K} \times$.

The following Proposition shows the maximal benefit that TEON can achieve over MUON.

Proposition 4.6 (Maximal Gain (Informal)). *Let $\{\mathbf{G}^{(k)}\}_{k=1}^K$ be the K layer gradients of the same matrix type, and let $\mathbf{u}_1^{(k)}, \mathbf{v}_1^{(k)}$ denote the leading left/right singular vectors of $\mathbf{G}^{(k)}$.*

- *If the leading right singular vectors are aligned across layers, i.e., $\langle \mathbf{v}_1^{(k)}, \mathbf{v}_1^{(k')} \rangle \rightarrow 1$ for all k, k' , then TEON with mode-1 orthogonalization approaches the maximal $\sqrt{K} \times$ improvement over MUON.*
- *If the leading left singular vectors are aligned across layers, i.e., $\langle \mathbf{u}_1^{(k)}, \mathbf{u}_1^{(k')} \rangle \rightarrow 1$ for all k, k' , then TEON with mode-2 orthogonalization approaches the maximal $\sqrt{K} \times$ improvement over MUON.*

4.1.3. IMPLICATION IN ALGORITHM DESIGN

Proposition 4.6 offers valuable insight on how to implement TEON in practice:

- **Implication 1: which layer to stack?** Proposition 4.6 shows that we should stack the gradient matrices that exhibit strongly aligned top left (or right) singular vectors. As will be shown in Section 6.2, such a strong alignment exists in the \mathbf{Q} , \mathbf{K} , and \mathbf{V} matrices of transformers.
- **Implication 2: how many layers to stack?** Theorem A.13 suggests that stacking more layers (larger K) achieves a greater potential maximum performance gain. Moreover, stacking more gradient matrices reduces the number of calls for SVD functions and thus the overall computational cost. However, Proposition 4.6 shows that to approach the best performance gains, all K matrices should have aligned top singular vectors. Therefore, the practical choice of K involves a trade-off, which is studied in Section 6.3.
- **Implication 3: along which mode to matricize the tensor?** According to Proposition 4.6, we should perform the mode-1 orthogonalization when the top right singular vectors (\mathbf{v}_1) have high similarity; and we should perform the mode-2 orthogonalization when the top left singular vectors (\mathbf{u}_1) have high similarity. The study in Section 6.1 shows that mode-1 orthogonalization works better in practice.

4.2. Sketch of Proofs

We provide a more detailed convergence analysis of TEON based on NTR (Kovalev, 2025). We follow the NTR conver-

gence bound derived by (Khaled et al., 2025).

Theorem 4.7 (NTR convergence under $\|\cdot\|$). *Under Assumptions 4.2–4.4 and suppose f is lower bounded by f^* , the iterates of (9) satisfy*

$$\mathbb{E} \left[\min_{t < T} \|\nabla f(\mathcal{W}_t)\|_* \right] \leq \frac{\Delta_0}{\eta T} + 3\sqrt{\frac{L\Delta_0}{T}} \cdot \frac{\mu}{1-\mu} + \frac{L\eta}{2} + L\eta \cdot \frac{\mu}{1-\mu} + \frac{2(1-\mu)\rho\sigma}{T} + \rho\sigma\sqrt{\frac{1-\mu}{1+\mu}}. \quad (10)$$

where $\Delta_0 := f(\mathcal{W}_0) - f^*$.

Considering the simplified setting ($\sigma = 0, \mu = 0$), minimizing Eq. (10) over η yields $\eta_* = \sqrt{\frac{2\Delta_0}{TL}}$ and the convergence guarantee

$$\min_{t < T} \|\nabla f(\mathcal{W}_t)\|_* \leq \sqrt{\frac{2L\Delta_0}{T}}. \quad (11)$$

Equation (11) shows that convergence comparisons reduce to comparing the dual norm and the smoothness constant L .

Sketch of Proof for Theorem 4.5. For $i \in \{1, 2\}$, we first derive the dual norm relation $\|\cdot\|_{\text{TEON}-i,*} \leq \|\cdot\|_{\text{MUON},*} \leq \sqrt{K} \|\cdot\|_{\text{TEON}-i,*}$ (proved in Appendix A.3) and smoothness constant relation $L_{\text{TEON}-i} \leq L_{\text{MUON}} \leq K L_{\text{TEON}-i}$ (proved in Appendix A.4). Plug in to Eq. (11), when $L_{\text{MUON}} \approx L_{\text{TEON}-i}$, the bounds of TEON and MUON matches, while in the best case $L_{\text{MUON}} = K \cdot L_{\text{TEON}-i}$ the bound of TEON can be up to $\sqrt{K} \times$ better than that of MUON. We provide detailed proof and derivation of convergence guarantees in Appendix A.5.

Sketch of Proof for Proposition 4.6. We first use the following lemma to show how the maximal gain could be achieved.

Lemma 4.8 (TEON’s maximal gain over MUON. Proved in Appendix A.6). *Let $\mathcal{G} = \nabla f(\mathcal{W}) \in \mathbb{R}^{m \times n \times K}$ have slices $\mathbf{G}^{(k)} \in \mathbb{R}^{m \times n}$.*

- **Mode-1 case.** *Assume each slice is rank-one, $\mathbf{G}^{(k)} = \mathbf{u}^{(k)}\mathbf{v}^\top$, where $\mathbf{v} \in \mathbb{R}^n$ is shared across all k , and the vectors $\{\mathbf{u}^{(k)}\}_{k=1}^K \subset \mathbb{R}^m$ are orthonormal. Then $L_{\text{MUON}} = \sqrt{K} L_{\text{TEON}-1}$.*
- **Mode-2 case.** *Assume each slice is rank-one, $\mathbf{G}^{(k)} = \mathbf{u}\mathbf{v}^{(k)\top}$, where $\mathbf{u} \in \mathbb{R}^m$ is shared across all k , and the vectors $\{\mathbf{v}^{(k)}\}_{k=1}^K \subset \mathbb{R}^n$ are orthonormal. Then $L_{\text{MUON}} = \sqrt{K} L_{\text{TEON}-2}$*

The assumption of rank-1 and shared singular vector in Lemma 4.8 characterizes an extreme case that achieves $\sqrt{K} \times$ improvement. In realistic training, layer-wise gradients are not rank-1 but typically *low-rank* (Gur-Ari et al.,

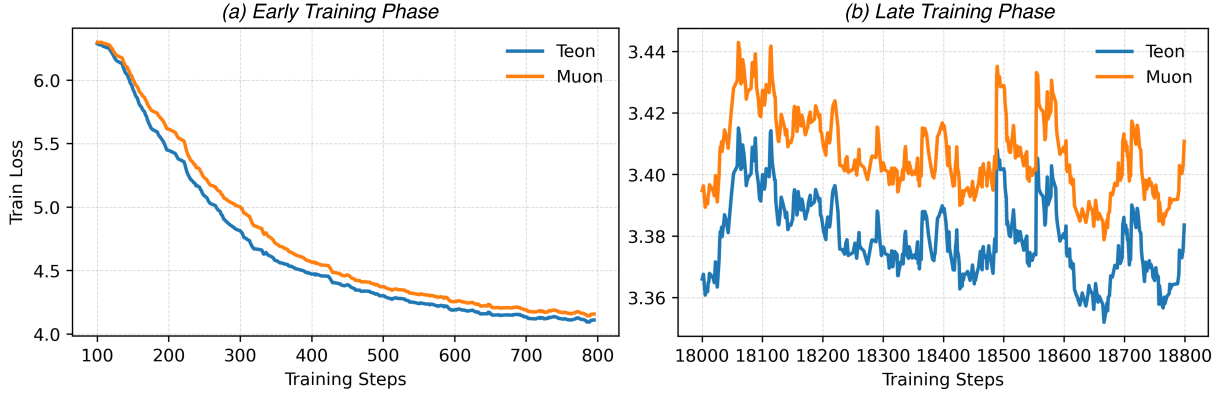


Figure 4. Training curves of GPT-Small on 10B tokens from the FineWeb dataset, comparing MUON and TEON using the original Newton–Schulz iteration with 5 steps. (a) At the beginning of training, TEON exhibits faster convergence, achieving lower training loss than MUON. (b) In the later stages, TEON continues to outperform MUON, achieving better final training loss.

2018; Zhao et al., 2024). In this case, TEON achieves a gain that is smaller than but close to $\sqrt{K} \times$, with the magnitude controlled by the alignment of the leading singular vectors across layers. This motivates the Proposition 4.6: stacking layers whose gradients exhibit strong top-singular-vector alignment as a practical criterion for applying cross-layer (mode-1 / mode-2) orthogonalization.

5. Experiment

We pre-train GPT-style and Llama-style models at different scales in this section. See hyperparameters in Appendix B. TEON and MUON have almost identical per-step computational cost in both memory and runtime. For this reason, we do not separately report memory usage or per-step runtime comparisons, and focus on optimization effectiveness in the following experiments.

5.1. Pre-training GPT-2

In this section, we evaluate TEON on GPT-style models, as summarized in Table 8. All models are pre-trained on the FineWeb dataset (Penedo et al., 2024), tokenized using the GPT tokenizer. Each model is trained on 10 billion tokens, with a vocabulary size of 50,257, a context length of 8,192, and a batch size of 512. Training is conducted on H100/A100 GPUs using mixed precision (bfloat16). Following the setup in (Amsel et al., 2025), we apply TEON (or MUON) to all parameters except for embeddings, unembeddings, normalization layers, and positional encodings, which are optimized using AdamW. To validate the robustness of TEON under different SVD approximation methods, we adopt 3 different methods in this section: You (You et al., 2019), Jordan (Jordan et al., 2024), and a more recent method, PolarExpress (Amsel et al., 2025).

As shown in Table 1, TEON consistently outperforms MUON across different model scales and orthogonalization approx-

Model	Ortho(·)	AdamW	Muon	TEON
GPT-Small	You		30.89	27.45
	Jordan	32.84	30.86	27.23
	PolarExpress		28.53	27.12
GPT-Base	You		22.55	21.16
	Jordan	29.33	22.26	21.15
	PolarExpress		21.64	20.92
GPT-Large	You		20.38	18.91
	Jordan	27.31	20.25	18.90
	PolarExpress		19.26	18.73

Table 1. Validation perplexity (PPL \downarrow) comparison among AdamW, MUON, and TEON on GPT-Small/Base/Large trained for 10B tokens. Ortho(·) applies only to MUON/TEON; all orthogonalization methods use 5 iterations.

Ortho(·)	Optimizer	Mean val PPL	Var
PolarExpress	TEON	27.15	0.0020
	Muon	28.57	0.0009
Jordan	TEON	27.31	0.0066
	Muon	31.00	0.0167
You	TEON	27.52	0.0026
	Muon	31.00	0.0241

Table 2. Mean and variance of validation perplexity across five runs for pre-training GPT-Small on 10 billion FineWeb tokens.

imation methods. Among all configurations, TEON combined with PolarExpress yields the lowest perplexity.

Due to resource constraints, we perform five independent runs only for GPT-Small trained on 10 billion tokens to estimate variance. The mean and variance of validation perplexity are reported in Table 2. The best single-run results for GPT-Small are reported separately in Table 1.

To further illustrate, we also present training curves in Figure 4. As shown in the figure, TEON exhibits superior performance in the early stages of training, demonstrating faster convergence compared to MUON. As training progresses,

Param	60M	130M	350M	1B
Tokens	1.1B	2.2B	6.4B	13.1B
AdamW	33.10	23.64	16.18	14.38
MUON(PolarExpress)	26.13	19.45	14.11	11.19
TEON(PolarExpress)	25.62	18.92	13.80	10.84

Table 3. Validation perplexity (PPL \downarrow) for LLaMA-style models pre-trained on FineWeb under different model scales.

TEON continues to maintain its advantage by achieving a lower final training loss.

5.2. Pre-training Llama

In addition to GPT-style models, we further validate our proposed methods by comparing against AdamW and MUON through pre-training LLaMA-style LLMs at scales ranging from 60M to 1B parameters on the FineWeb dataset. Model configurations are summarized in Table 13.

Following the compute-optimal token-to-parameter ratios (Hoffmann et al., 2022), we train 60M, 130M, 350M, and 1B parameter models on 1.1B, 2.2B, 6.4B, and 13.1B tokens respectively. All models use a sequence length of 1,024, batch size of 512 and a vocabulary size of 32,000, tokenized with the LLaMA-2 tokenizer. Consistent with Section 5.1, training is conducted on H100/A100 GPUs using mixed precision. See more hyperparameters in Appendix B. As shown in Table 3, TEON consistently achieves the best overall performance at different scales.

6. Ablation Study

As mentioned in Section 3.2, the implementation of our TEON algorithm needs proper choices of some hyperparameters and stacking configurations. Section 4.1.3 has already provided some theoretical guidance. This section provides a detailed ablation study, which further explains how these choices are made in practice.

6.1. Ablation for Orthogonalization Mode

Proposition 4.6 suggests two options for orthogonalization: (1) mode-1 orthogonalization when the top right singular vectors exhibit high similarity, and (2) mode-2 orthogonalization when the top left singular vectors are more aligned. In order to know which option works better in practice, we pre-train a GPT-Small model on 1 billion FineWeb tokens and track the evolution of the top singular vectors similarity of the momentum gradients across two consecutive layers during MUON training.

As shown in Figure 5a, the momentum matrices exhibit strong alignment in their top right singular vectors, whereas their top left singular vectors remain largely orthogonal.

		SVD	PolarExpress
MUON	/	36.43	36.70
TEON	Mode-1	34.29	34.94
TEON	Mode-2	34.54	35.17

Table 4. Validation perplexity (PPL \downarrow) of MUON and TEON with different orthogonalization modes.

Method	QKV	O	MLP1	MLP2	Val PPL \downarrow
MUON	\times	\times	\times	\times	36.43
	✓	\times	\times	\times	34.29
	✓	✓	\times	\times	34.37
	✓	\times	\times	✓	34.53
	✓	\times	✓	\times	34.53
TEON	✓	✓	✓	\times	34.59
	✓	✓	✓	\times	34.65
	✓	✓	\times	✓	34.71
	✓	\times	✓	✓	34.72

Table 5. Ablation of layer grouping strategies for TEON. All the experiments in this table use exact SVD as their $Ortho(\cdot)$

This implies that TEON with mode-1 orthogonalization is expected to achieve more significant gains over MUON. This is consistent with our training results in Table 4: mode-1 choice yields the highest performance improvement.

6.2. Ablation for Layer Type in Stacking

In the algorithm implementation, we must decide which layers to stack. Proposition 4.6 suggests stacking gradient matrices whose top singular vectors are strongly aligned. To verify this, we measure cross-layer singular vector similarity under the same setup as Table 4, with results shown in Figure 5b. Compared to same-type groupings in Figure 5a, the similarities among Q , K , and V gradients are weaker and less stable, indicating that stacking gradients from the same layer type yields better alignment.

We further study how different stacking choices affect performance. To isolate the effect of stacking, we use exact SVD to compute UV^\top and consider stacking gradients from attention projections (Q , K , V), the attention output projection (O), and the two MLP sublayers. As shown in Table 5, stacking only QKV achieves the largest improvement. We attribute this to the functional asymmetry in Transformers: prior work (Dong et al., 2025) shows that MLP layers mainly store heterogeneous memorization, while attention layers share a common retrieval-oriented role.

In practice, TEON relies on approximate SVD. Stacking MLP gradients often produces highly rectangular matrices with extreme aspect ratios, which degrade the accuracy and numerical stability of SVD approximations. Table 6 shows that TEON gains diminish when using approximate SVD, especially for less accurate methods and when stacking MLP2 gradients. PolarExpress performs best and is closest to ex-

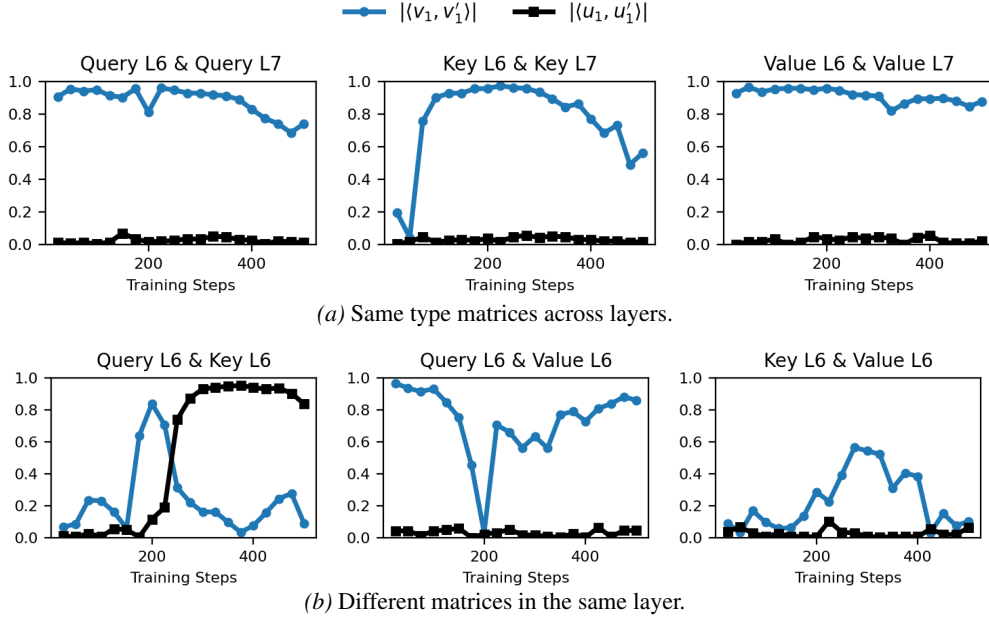


Figure 5. We perform SVD on the momentum terms M_t and plot the inner product between top singular vectors of consecutive layer pairs. For QKV matrices, the top right singular vectors are aligned while top left singular vectors remain almost orthogonal. We provide the plot for all matrices pairs in Appendix C.1.

Ortho(·)	Method	Val PPL ↓
SVD	MUON	36.43
	TEON (QKV)	34.29
	TEON (MLP2+QKV)	34.53
You	MUON	38.95
	TEON (QKV)	37.43
	TEON (MLP2+QKV)	37.83
Jordan	MUON	38.59
	TEON (QKV)	37.45
	TEON (MLP2+QKV)	38.01
PolarExpress	MUON	36.70
	TEON (QKV)	34.94
	TEON (MLP2+QKV)	35.52

Table 6. Comparison between MUON and TEON (QKV vs. QKV + MLP2) using the same SVD approximation method.

act SVD, while other methods suffer larger performance gaps due to ill-conditioned matrices. Therefore, we recommend stacking only QKV gradients in TEON for optimal performance.

6.3. Ablation for Layer Number

To study the trade-off caused by the stacking layer number (K) mentioned in Section 4.1.3, we conduct a controlled experiment on GPT-Small (with 12 layers). As shown in Table 7, TEON achieves the best performance at $K = 2$. Increasing K gradually degrades performance under exact SVD. This suggests that as more layers are stacked, it becomes harder for all stacked gradient matrices to have similar top singular vectors, making it difficult to reach the

	SVD	PolarExpress
MUON	/	36.43
	34.29	34.94
	34.49	35.35
TEON	$K=6$	34.75
	$K=12$	34.76
		36.55

Table 7. Validation perplexity (PPL ↓) of TEON with different stacking group sizes K .

best-case gain in Proposition 4.6.

In practice, orthogonalization is approximated for efficiency. When using PolarExpress, this degradation is further amplified, as larger K also leads to less accurate SVD approximations due to the increasing unbalanced tensor shape.

7. Conclusion

In this work, we have proposed TEON, a tensor-level generalization of the MUON optimizer. By modeling stacking multiple gradient matrices as higher-order tensors, TEON improves the training performance of Transformer models. We have provided theoretical analysis to show the better convergence properties of TEON over MUON, which has been experimentally observed in the pre-training experiments of GPT-2 and LLaMA-type models. These theoretical results also provide valuable guidance for practical implementation, which has been validated through extensive ablation studies.

Impact Statement

This work focuses on improving the optimization methods for large-scale neural network pre-training. By extending gradient orthogonalization to structured tensors, Our proposed method TEON enables more effective use of cross-layer gradient information, which can improve training efficiency for large models. Such efficiency improvements may help lower the resource and energy costs associated with pre-training foundation models. The proposed method is a general optimization technique, evaluated using publicly available models and datasets, and does not introduce new model capabilities or inherently harmful functionalities. We do not foresee any immediate negative societal impacts arising from this work.

References

Achiam, J., Adler, S., Agarwal, S., Ahmad, L., Akkaya, I., Aleman, F. L., Almeida, D., Altenschmidt, J., Altman, S., Anadkat, S., et al. Gpt-4 technical report. *arXiv preprint arXiv:2303.08774*, 2023.

Amari, S.-I. Natural gradient works efficiently in learning. *Neural computation*, 10(2):251–276, 1998.

Amsel, N., Persson, D., Musco, C., and Gower, R. M. The polar express: Optimal matrix sign methods and their application to the muon algorithm. *arXiv preprint arXiv:2505.16932*, 2025.

Bernstein, J. Deriving muon, 2025. URL <https://jeremybernste.in/writing/deriving-muon>.

Cesista, F. L., Jiacheng, Y., and Jordan, K. Squeezing 1-2 URL <https://leloykun.github.io/ponder/muon-opt-coeffs/>.

Ding, D., Ju, Z., Leng, Y., Liu, S., Liu, T., Shang, Z., Shen, K., Song, W., Tan, X., Tang, H., et al. Kimi-audio technical report. *arXiv preprint arXiv:2504.18425*, 2025.

Dong, Y., Noci, L., Khodak, M., and Li, M. Attention retrieves, mlp memorizes: Disentangling trainable components in the transformer. *arXiv preprint arXiv:2506.01115*, 2025.

Grattafiori, A., Dubey, A., Jauhri, A., Pandey, A., Kadian, A., Al-Dahle, A., Letman, A., Mathur, A., Schelten, A., Vaughan, A., et al. The llama 3 herd of models. *arXiv preprint arXiv:2407.21783*, 2024.

Gur-Ari, G., Roberts, D. A., and Dyer, E. Gradient descent happens in a tiny subspace. *arXiv preprint arXiv:1812.04754*, 2018.

Han, A., Li, J., Huang, W., Hong, M., Takeda, A., Jawanpuria, P. K., and Mishra, B. Sltrain: a sparse plus low rank approach for parameter and memory efficient pretraining. *Advances in Neural Information Processing Systems*, 37: 118267–118295, 2024.

Higham, N. J. *Functions of matrices: theory and computation*. SIAM, 2008.

Hoffmann, J., Borgeaud, S., Mensch, A., Buchatskaya, E., Cai, T., Rutherford, E., de Las Casas, D., Hendricks, L. A., Welbl, J., Clark, A., et al. Training compute-optimal large language models. In *Proceedings of the 36th International Conference on Neural Information Processing Systems*, pp. 30016–30030, 2022.

Hwang, D. Fadam: Adam is a natural gradient optimizer using diagonal empirical fisher information. *arXiv preprint arXiv:2405.12807*, 2024.

Jordan, K., Jin, Y., Boza, V., You, J., Cesista, F., Newhouse, L., and Bernstein, J. Muon: An optimizer for hidden layers in neural networks, 2024. URL <https://kellerjordan.github.io/posts/muon/>.

Kaplan, J., McCandlish, S., Henighan, T., Brown, T. B., Chess, B., Child, R., Gray, S., Radford, A., Wu, J., and Amodei, D. Scaling laws for neural language models. *arXiv preprint arXiv:2001.08361*, 2020.

Khaled, A., Ozkara, K., Yu, T., Hong, M., and Park, Y. Muonbp: Faster muon via block-periodic orthogonalization. *arXiv preprint arXiv:2510.16981*, 2025.

Kingma, D. P. Adam: A method for stochastic optimization. *arXiv preprint arXiv:1412.6980*, 2014.

Kolda, T. G. and Bader, B. W. Tensor decompositions and applications. *SIAM review*, 51(3):455–500, 2009.

Kovalev, D. Understanding gradient orthogonalization for deep learning via non-euclidean trust-region optimization. *arXiv preprint arXiv:2503.12645*, 2025.

Kumar, T., Ankner, Z., Spector, B. F., Bordelon, B., Muenninghoff, N., Paul, M., Pehlevan, C., Re, C., and Raghunathan, A. Scaling laws for precision. In *The Thirteenth International Conference on Learning Representations*, 2025. URL <https://openreview.net/forum?id=wg1PCg3CUP>.

Li, X. Black box lie group preconditioners for sgd, 2022. URL <https://arxiv.org/abs/2211.04422>.

Li, X.-L. Preconditioned stochastic gradient descent. *IEEE Transactions on Neural Networks and Learning Systems*, 29(5):1454–1466, May 2018a. ISSN 2162-2388. doi: 10.1109/tnnls.2017.2672978. URL <http://dx.doi.org/10.1109/TNNLS.2017.2672978>.

Li, X.-L. Preconditioner on matrix lie group for sgd, 2018b. URL <https://arxiv.org/abs/1809.10232>.

Li, X.-L. Stochastic hessian fittings with lie groups, 2024. URL <https://arxiv.org/abs/2402.11858>.

Li, Z., Liu, L., Liang, C., Chen, W., and Zhao, T. Normuon: Making muon more efficient and scalable. *arXiv preprint arXiv:2510.05491*, 2025.

Liu, A., Feng, B., Xue, B., Wang, B., Wu, B., Lu, C., Zhao, C., Deng, C., Zhang, C., Ruan, C., et al. Deepseek-v3 technical report. *arXiv preprint arXiv:2412.19437*, 2024a.

Liu, H., Li, Z., Hall, D. L. W., Liang, P., and Ma, T. Sophia: A scalable stochastic second-order optimizer for language model pre-training. In *The Twelfth International Conference on Learning Representations*, 2024b. URL <https://openreview.net/forum?id=3xHDeA8Noi>.

Liu, J., Su, J., Yao, X., Jiang, Z., Lai, G., Du, Y., Qin, Y., Xu, W., Lu, E., Yan, J., et al. Muon is scalable for llm training. *arXiv preprint arXiv:2502.16982*, 2025a.

Liu, Z., Zhang, R., Wang, Z., Yan, M., Yang, Z., Hovland, P. D., Nicolae, B., Cappello, F., Tang, S., and Zhang, Z. Cola: Compute-efficient pre-training of llms via low-rank activation. In *Proceedings of the 2025 Conference on Empirical Methods in Natural Language Processing*, pp. 4627–4645, 2025b.

Loshchilov, I. and Hutter, F. Decoupled weight decay regularization. *arXiv preprint arXiv:1711.05101*, 2017.

Mehmood, F., Ahmad, S., and Whangbo, T. K. An efficient optimization technique for training deep neural networks. *Mathematics*, 11(6):1360, 2023.

Penedo, G., Kydlíček, H., Lozhkov, A., Mitchell, M., Raffel, C. A., Von Werra, L., Wolf, T., et al. The fineweb datasets: Decanting the web for the finest text data at scale. *Advances in Neural Information Processing Systems*, 37: 30811–30849, 2024.

Pethick, T., Xie, W., Antonakopoulos, K., Zhu, Z., Silveti-Falls, A., and Cevher, V. Training deep learning models with norm-constrained lmos, 2025. URL <https://arxiv.org/abs/2502.07529>.

Pooladzandi, O. and Li, X.-L. Curvature-informed sgd via general purpose lie-group preconditioners, 2024. URL <https://arxiv.org/abs/2402.04553>.

Team, G., Anil, R., Borgeaud, S., Alayrac, J.-B., Yu, J., Soricut, R., Schalkwyk, J., Dai, A. M., Hauth, A., Millican, K., et al. Gemini: a family of highly capable multimodal models. *arXiv preprint arXiv:2312.11805*, 2023.

Team, K., Bai, Y., Bao, Y., Chen, G., Chen, J., Chen, N., Chen, R., Chen, Y., Chen, Y., Chen, Y., et al. Kimi k2: Open agentic intelligence. *arXiv preprint arXiv:2507.20534*, 2025a.

Team, K., Du, A., Yin, B., Xing, B., Qu, B., Wang, B., Chen, C., Zhang, C., Du, C., Wei, C., et al. Kimi-vl technical report. *arXiv preprint arXiv:2504.07491*, 2025b.

Vyas, N., Morwani, D., Zhao, R., Shapira, I., Brandfonbrener, D., Janson, L., and Kakade, S. M. SOAP: Improving and stabilizing shampoo using adam. In *The Thirteenth International Conference on Learning Representations*, 2025. URL <https://openreview.net/forum?id=IDxZhXrpNf>.

You, Y., Li, J., Reddi, S., Hseu, J., Kumar, S., Bhojanapalli, S., Song, X., Demmel, J., Keutzer, K., and Hsieh, C.-J. Large batch optimization for deep learning: Training bert in 76 minutes. *arXiv preprint arXiv:1904.00962*, 2019.

Yuan, H., Liu, Y., Wu, S., Zhou, X., and Gu, Q. Mars: Unleashing the power of variance reduction for training large models, 2024.

Zeng, A., Lv, X., Zheng, Q., Hou, Z., Chen, B., Xie, C., Wang, C., Yin, D., Zeng, H., Zhang, J., et al. Glm-4.5: Agentic, reasoning, and coding (arc) foundation models. *arXiv preprint arXiv:2508.06471*, 2025.

Zhang, R., Liu, Z., Wang, Z., and Zhang, Z. Lax: Boosting low-rank training of foundation models via latent crossing. *arXiv preprint arXiv:2505.21732*, 2025.

Zhao, J., Zhang, Z., Chen, B., Wang, Z., Anandkumar, A., and Tian, Y. Galore: Memory-efficient llm training by gradient low-rank projection. *arXiv preprint arXiv:2403.03507*, 2024.

A. Detailed Proofs for Section 4

A.1. Tensor norms for MUON and TEON

Throughout, let $\mathcal{X} \in \mathbb{R}^{m \times n \times K}$ with slices $\mathcal{X}[:, :, k] = X^{(k)} \in \mathbb{R}^{m \times n}$ for $k \in [K]$, and let $\mathcal{M}_i(\cdot)$ denote the mode- i matricization.

Definition A.1 (TEON norm family). For each $i \in \{1, 2, 3\}$, define the TEON norm and its dual by

$$\|\mathcal{X}\|_{\text{TEON}-i} := \|\mathcal{M}_i(\mathcal{X})\|_{\text{op}}, \quad (12)$$

and

$$\|\mathcal{X}\|_{\text{TEON}-i,*} := \|\mathcal{M}_i(\mathcal{X})\|_{*}. \quad (13)$$

Definition A.2 (MUON norm). Define the layer-wise MUON norm and its dual by

$$\|\mathcal{X}\|_{\text{MUON}} := \max_{k \in [K]} \|X^{(k)}\|_{\text{op}}, \quad (14)$$

and

$$\|\mathcal{X}\|_{\text{MUON},*} := \sum_{k=1}^K \|X^{(k)}\|_{*}. \quad (15)$$

Since these norms are induced by matrix operator norms, they are well-defined norms on $\mathbb{R}^{m \times n \times K}$.

The dual of TEON norm and MUON norm are derived as follows:

Lemma A.3 (Dual of $\|\cdot\|_{\text{TEON}-i}$). Fix $i \in \{1, 2, 3\}$. The dual of $\|\cdot\|_{\text{TEON}-i}$ is $\|\cdot\|_{\text{TEON}-i,*}$ as defined in (13), i.e.,

$$(\|\cdot\|_{\text{TEON}-i})_*(\mathcal{X}) = \|\mathcal{M}_i(\mathcal{X})\|_{*}. \quad (16)$$

Proof. By definition of the dual norm and invariance of the Frobenius inner product under matricization,

$$\begin{aligned} (\|\cdot\|_{\text{TEON}-i})_*(\mathcal{X}) &= \sup_{\|\mathcal{Y}\|_{\text{TEON}-i} \leq 1} \langle \mathcal{X}, \mathcal{Y} \rangle = \sup_{\|\mathcal{M}_i(\mathcal{Y})\|_{\text{op}} \leq 1} \langle \mathcal{M}_i(\mathcal{X}), \mathcal{M}_i(\mathcal{Y}) \rangle_F \\ &= \sup_{\|Y\|_{\text{op}} \leq 1} \langle \mathcal{M}_i(\mathcal{X}), Y \rangle_F = \|\mathcal{M}_i(\mathcal{X})\|_{*}, \end{aligned} \quad (17)$$

where the last equality uses that the dual of $\|\cdot\|_{\text{op}}$ is $\|\cdot\|_{*}$. \square

Lemma A.4 (Dual of $\|\cdot\|_{\text{MUON}}$). The dual of $\|\cdot\|_{\text{MUON}}$ in (14) is $\|\cdot\|_{\text{MUON},*}$ in (15), i.e.,

$$(\|\cdot\|_{\text{MUON}})_*(\mathcal{X}) = \sum_{k=1}^K \|X^{(k)}\|_{*}. \quad (18)$$

Proof. By definition, the constraint $\|\mathcal{Y}\|_{\text{MUON}} \leq 1$ is equivalent to $\|Y^{(k)}\|_{\text{op}} \leq 1$ for all $k \in [K]$. Hence

$$\begin{aligned} (\|\cdot\|_{\text{MUON}})_*(\mathcal{X}) &= \sup_{\|\mathcal{Y}\|_{\text{MUON}} \leq 1} \langle \mathcal{X}, \mathcal{Y} \rangle = \sup_{\max_k \|Y^{(k)}\|_{\text{op}} \leq 1} \sum_{k=1}^K \langle X^{(k)}, Y^{(k)} \rangle_F \\ &= \sum_{k=1}^K \sup_{\|Y^{(k)}\|_{\text{op}} \leq 1} \langle X^{(k)}, Y^{(k)} \rangle_F = \sum_{k=1}^K \|X^{(k)}\|_{*}, \end{aligned} \quad (19)$$

where the last equality again uses that the dual of $\|\cdot\|_{\text{op}}$ is $\|\cdot\|_{*}$. \square

Lemma A.5 (Norm equivalence constants for MUON and TEON). The norm equivalence constants in Assumption 4.4 for the MUON norm and the TEON norms (mode- i , $i \in \{1, 2\}$) are equal to one. That is,

$$\rho_{\text{MUON}} = 1, \quad \rho_{\text{TEON}-i} = 1 \quad (i = 1, 2).$$

Proof. Let $\mathcal{X} \in \mathbb{R}^{A \times B \times K}$ with slices $\mathcal{X}[:, :, k] = X^{(k)}$.

Muon. By definition,

$$\|\mathcal{X}\|_{\text{MUON}} := \max_{k \in [K]} \|X^{(k)}\|_{\text{op}}.$$

For each slice, $\|X^{(k)}\|_{\text{op}} \leq \|X^{(k)}\|_F$. Hence,

$$\|\mathcal{X}\|_{\text{MUON}} \leq \max_k \|X^{(k)}\|_F \leq \left(\sum_{k=1}^K \|X^{(k)}\|_F^2 \right)^{1/2} = \|\mathcal{X}\|_F,$$

which implies $\rho_{\text{MUON}} = 1$.

Teon (mode- i , $i = 1, 2$). By definition,

$$\|\mathcal{X}\|_{\text{TEON-}i} := \|\mathcal{M}_i(\mathcal{X})\|_{\text{op}}.$$

The operator norm of any matrix is upper bounded by its Frobenius norm, so

$$\|\mathcal{X}\|_{\text{TEON-}i} = \|\mathcal{M}_i(\mathcal{X})\|_{\text{op}} \leq \|\mathcal{M}_i(\mathcal{X})\|_F.$$

Since matricization preserves the Frobenius norm, $\|\mathcal{M}_i(\mathcal{X})\|_F = \|\mathcal{X}\|_F$, we obtain

$$\|\mathcal{X}\|_{\text{TEON-}i} \leq \|\mathcal{X}\|_F,$$

which implies $\rho_{\text{TEON-}i} = 1$. \square

A.2. TEON/MUON step as steepest descent

We show that TEON and MUON updates are the exact solutions to the NTR linearized trust-region subproblem under their respective norms. Throughout this subsection, $\mathcal{G} \in \mathbb{R}^{m \times n \times K}$ denotes the stacked gradient tensor, and $\langle \cdot, \cdot \rangle$ denotes the standard Frobenius inner product on tensors (equivalently, the Euclidean inner product after vectorization). We write $\mathcal{M}_i(\cdot)$ for the mode- i matricization and $\mathcal{M}_i^{-1}(\cdot)$ for its inverse.

Proposition A.6 (TEON step as steepest descent / trust-region step). *Fix $i \in \{1, 2, 3\}$ and consider the trust-region subproblem*

$$\min_{\Delta \mathcal{W}: \|\Delta \mathcal{W}\|_{\text{TEON-}i} \leq \eta} \langle \mathcal{G}, \Delta \mathcal{W} \rangle, \quad (20)$$

where $\|\mathcal{X}\|_{\text{TEON-}i} := \|\mathcal{M}_i(\mathcal{X})\|_{\text{op}}$. Let $\mathcal{M}_i(\mathcal{G}) = U \Sigma V^\top$ be a (thin) SVD. Then an optimal solution is

$$\Delta \mathcal{W} = -\eta \mathcal{M}_i^{-1}(U V^\top). \quad (21)$$

Proof. Fix $i \in \{1, 2, 3\}$. By definition of $\|\cdot\|_{\text{TEON-}i}$ and invariance of the Frobenius inner product under matricization,

$$\arg \min_{\|\Delta \mathcal{W}\|_{\text{TEON-}i} \leq \eta} \langle \mathcal{G}, \Delta \mathcal{W} \rangle = \mathcal{M}_i^{-1} \left(\arg \min_{\|\mathcal{M}_i(\Delta \mathcal{W})\|_{\text{op}} \leq \eta} \langle \mathcal{M}_i(\mathcal{G}), \mathcal{M}_i(\Delta \mathcal{W}) \rangle_F \right) \quad (22)$$

$$= \mathcal{M}_i^{-1} \left(\arg \min_{\|Y\|_{\text{op}} \leq \eta} \langle \mathcal{M}_i(\mathcal{G}), Y \rangle_F \right). \quad (23)$$

Let $Y = \eta \tilde{Y}$ with $\|\tilde{Y}\|_{\text{op}} \leq 1$. Then

$$\arg \min_{\|Y\|_{\text{op}} \leq \eta} \langle \mathcal{M}_i(\mathcal{G}), Y \rangle_F = -\eta \arg \max_{\|\tilde{Y}\|_{\text{op}} \leq 1} \langle \mathcal{M}_i(\mathcal{G}), \tilde{Y} \rangle_F. \quad (24)$$

If $\mathcal{M}_i(\mathcal{G}) = U \Sigma V^\top$ is a thin SVD, then the maximizer of $\max_{\|\tilde{Y}\|_{\text{op}} \leq 1} \langle \mathcal{M}_i(\mathcal{G}), \tilde{Y} \rangle_F$ is $\tilde{Y}^* = U V^\top$ (a standard duality fact: the dual of $\|\cdot\|_{\text{op}}$ is $\|\cdot\|_*$). Substituting \tilde{Y}^* into (24) and then into (23)–(22) yields $\Delta \mathcal{W} = -\eta \mathcal{M}_i^{-1}(U V^\top)$. \square

Proposition A.7 (MUON step as steepest descent / trust-region step). *Consider the trust-region subproblem*

$$\min_{\Delta\mathcal{W}: \|\Delta\mathcal{W}\|_{\text{MUON}} \leq \eta} \langle \mathcal{G}, \Delta\mathcal{W} \rangle, \quad (25)$$

where the MUON norm is $\|\mathcal{X}\|_{\text{MUON}} := \max_{k \in [K]} \|\mathcal{X}[:, :, k]\|_{\text{op}}$. For each slice, let $\mathcal{G}[:, :, k] = G^{(k)} = U^{(k)}\Sigma^{(k)}(V^{(k)})^\top$ be a (thin) SVD. Then an optimal solution has slices

$$\Delta\mathcal{W}[:, :, k] = -\eta U^{(k)}(V^{(k)})^\top, \quad \forall k \in [K]. \quad (26)$$

Proof. By definition of $\|\cdot\|_{\text{MUON}}$, the constraint $\|\Delta\mathcal{W}\|_{\text{MUON}} \leq \eta$ is equivalent to $\|\Delta\mathcal{W}[:, :, k]\|_{\text{op}} \leq \eta$ for all $k \in [K]$. Moreover, $\langle \mathcal{G}, \Delta\mathcal{W} \rangle = \sum_{k=1}^K \langle G^{(k)}, \Delta W^{(k)} \rangle_F$. Therefore (25) decouples across layers:

$$\min_{\|\Delta\mathcal{W}\|_{\text{MUON}} \leq \eta} \langle \mathcal{G}, \Delta\mathcal{W} \rangle = \sum_{k=1}^K \min_{\|\Delta W^{(k)}\|_{\text{op}} \leq \eta} \langle G^{(k)}, \Delta W^{(k)} \rangle_F. \quad (27)$$

Each summand is the matrix trust-region subproblem under $\|\cdot\|_{\text{op}}$. Let $G^{(k)} = U^{(k)}\Sigma^{(k)}(V^{(k)})^\top$ be a thin SVD. By the same duality argument as in Proposition A.6, the minimizer is $\Delta W^{(k)} = -\eta U^{(k)}(V^{(k)})^\top$. Stacking these slices yields (26). \square

A.3. Proof for comparability of the norm and dual norm of TEON and MUON

Lemma A.8 (Comparability for $i = 1$). *For any $\mathcal{X} \in \mathbb{R}^{m \times n \times K}$,*

$$\|\mathcal{X}\|_{\text{MUON}} \leq \|\mathcal{X}\|_{\text{TEON-1}} \leq \sqrt{K} \|\mathcal{X}\|_{\text{MUON}}. \quad (28)$$

Proof. Write $\mathcal{M}_1(\mathcal{X}) = [X^{(1)}, \dots, X^{(K)}] \in \mathbb{R}^{A \times (BK)}$.

Lower bound. Fix $k \in [K]$. For any unit vector $v \in \mathbb{R}^B$, let $z \in \mathbb{R}^{BK}$ be the unit block vector whose k -th block equals v and all other blocks are zero. Then $\mathcal{M}_1(\mathcal{X})z = X^{(k)}v$, hence

$$\|\mathcal{M}_1(\mathcal{X})\|_{\text{op}} = \sup_{\|z\|_2=1} \|\mathcal{M}_1(\mathcal{X})z\|_2 \geq \sup_{\|v\|_2=1} \|X^{(k)}v\|_2 = \|X^{(k)}\|_{\text{op}}.$$

Taking the maximum over k gives $\|\mathcal{X}\|_{\text{TEON-1}} \geq \|\mathcal{X}\|_{\text{MUON}}$.

Upper bound. Let $z \in \mathbb{R}^{BK}$ be any unit vector with blocks $z = [z_1^\top \cdots z_K^\top]^\top$, $z_k \in \mathbb{R}^B$. Then $\mathcal{M}_1(\mathcal{X})z = \sum_{k=1}^K X^{(k)}z_k$, and

$$\begin{aligned} \|\mathcal{M}_1(\mathcal{X})z\|_2 &\leq \sum_{k=1}^K \|X^{(k)}z_k\|_2 \leq \sum_{k=1}^K \|X^{(k)}\|_{\text{op}} \|z_k\|_2 \\ &\leq \left(\sum_{k=1}^K \|X^{(k)}\|_{\text{op}}^2 \right)^{1/2} \left(\sum_{k=1}^K \|z_k\|_2^2 \right)^{1/2} = \left(\sum_{k=1}^K \|X^{(k)}\|_{\text{op}}^2 \right)^{1/2}. \end{aligned}$$

Taking $\sup_{\|z\|_2=1}$ yields

$$\|\mathcal{M}_1(\mathcal{X})\|_{\text{op}} \leq \left(\sum_{k=1}^K \|X^{(k)}\|_{\text{op}}^2 \right)^{1/2} \leq \sqrt{K} \max_k \|X^{(k)}\|_{\text{op}} = \sqrt{K} \|\mathcal{X}\|_{\text{MUON}}.$$

\square

Lemma A.9 (Comparability for $i = 2$). *For any $\mathcal{X} \in \mathbb{R}^{m \times n \times K}$,*

$$\|\mathcal{X}\|_{\text{MUON}} \leq \|\mathcal{X}\|_{\text{TEON-2}} \leq \sqrt{K} \|\mathcal{X}\|_{\text{MUON}}. \quad (29)$$

Proof. Under the standard mode-2 unfolding, $\mathcal{M}_2(\mathcal{X}) = [(X^{(1)})^\top \cdots (X^{(K)})^\top] \in \mathbb{R}^{B \times (AK)}$, which is again a horizontal concatenation of K blocks. The proof is identical to Lemma A.8, using $\|(X^{(k)})^\top\|_{\text{op}} = \|X^{(k)}\|_{\text{op}}$. \square

Lemma A.10 (Dual-norm comparability). *Let $\|\cdot\|_a$ and $\|\cdot\|_b$ be norms on an inner-product space with duals $\|\cdot\|_{a,*}$ and $\|\cdot\|_{b,*}$. If there exist $\alpha, \beta > 0$ such that for all x ,*

$$\alpha\|x\|_a \leq \|x\|_b \leq \beta\|x\|_a,$$

then for all g ,

$$\frac{1}{\beta}\|g\|_{a,*} \leq \|g\|_{b,*} \leq \frac{1}{\alpha}\|g\|_{a,*}.$$

Corollary A.11 (Dual comparability for $i = 1, 2$). *For $i \in \{1, 2\}$ and all \mathcal{X} ,*

$$\|\mathcal{X}\|_{\text{TEON}-i,*} \leq \|\mathcal{X}\|_{\text{MUON},*} \leq \sqrt{K} \|\mathcal{X}\|_{\text{TEON}-i,*}. \quad (30)$$

Proof. Apply Lemma A.10 with $\|\cdot\|_a = \|\cdot\|_{\text{TEON}-i}$, $\|\cdot\|_b = \|\cdot\|_{\text{MUON}}$, and use Lemmas A.8–A.9. \square

A.4. Proof for comparability of smoothness constants

Lemma A.12 (Smoothness constant comparability). *Let L_{MUON} be the smoothness constant under $\|\cdot\|_{\text{MUON}}$ and $L_{\text{TEON}-i}$ the smoothness constant under $\|\cdot\|_{\text{TEON}-i}$. Then for $i \in \{1, 2\}$,*

$$L_{\text{TEON}-i} \leq L_{\text{MUON}} \leq K \cdot L_{\text{TEON}-i}, \quad (31)$$

Proof. We use the smoothness definition in Assumption 4.2 from the body. For any $\mathcal{X} \neq \mathcal{Y}$, define the ratio

$$R(\mathcal{X}, \mathcal{Y}) := \frac{\|\nabla f(\mathcal{X}) - \nabla f(\mathcal{Y})\|_*}{\|\mathcal{X} - \mathcal{Y}\|}.$$

Then $L = \sup_{\mathcal{X} \neq \mathcal{Y}} R(\mathcal{X}, \mathcal{Y})$.

For $i \in \{1, 2\}$, Lemmas A.8–A.9 give $\|\cdot\|_{\text{MUON}} \leq \|\cdot\|_{\text{TEON}-i} \leq \sqrt{K} \|\cdot\|_{\text{MUON}}$, and Corollary A.11 gives $\|\cdot\|_{\text{TEON}-i,*} \leq \|\cdot\|_{\text{MUON},*} \leq \sqrt{K} \|\cdot\|_{\text{TEON}-i,*}$. Therefore, for any $\mathcal{X} \neq \mathcal{Y}$,

$$R_{\text{TEON}-i}(\mathcal{X}, \mathcal{Y}) \leq R_{\text{MUON}}(\mathcal{X}, \mathcal{Y}) \leq K \cdot R_{\text{TEON}-i}(\mathcal{X}, \mathcal{Y}),$$

and taking suprema yields (31). \square

A.5. Proof of Theorem A.13

Theorem A.13 (Convergence Bound). *Consider minimizing $f(\mathcal{W})$, $\mathcal{W} \in \mathbb{R}^{m \times n \times K}$ and suppose f is lower bounded by f^* . $\Delta_0 = (f(\mathcal{W}_0) - f^*)$. Define the best iterates of MUON and TEON as $\tau_{\text{MUON}} := \arg \min_{0 \leq t < T} \|\nabla f(\mathcal{W}_t)\|_{\text{MUON},*}$ and $\tau_{\text{TEON}} := \arg \min_{0 \leq t < T} \|\nabla f(\mathcal{W}_t)\|_{\text{TEON},*}$.*

Under the same TEON norm (c.f. Definition 4.1), the convergence bounds satisfy:

$$\begin{aligned} \|\nabla f(\mathcal{W}_{\tau_{\text{TEON}}})\|_{\text{TEON},*} &\leq \sqrt{\frac{2L_{\text{TEON}}\Delta_0}{T}}, \\ \|\nabla f(\mathcal{W}_{\tau_{\text{MUON}}})\|_{\text{TEON},*} &\leq \sqrt{\frac{2L_{\text{MUON}}\Delta_0}{T}} \\ &\leq \sqrt{K} \sqrt{\frac{2L_{\text{TEON}}\Delta_0}{T}}. \end{aligned} \quad (32)$$

Proof. Define the best iterates of MUON and TEON as $\tau_{\text{MUON}} := \arg \min_{0 \leq t < T} \|\nabla f(\mathcal{W}_t)\|_{\text{MUON},*}$ and $\tau_{\text{TEON}} := \arg \min_{0 \leq t < T} \|\nabla f(\mathcal{W}_t)\|_{\text{TEON},*}$.

From the NTR convergence guarantee under the $\|\cdot\|_{\text{TEON}}$ norm and the corresponding smoothness constant L_{TEON} , it follows that

$$\|\nabla f(\mathcal{W}_{\tau_{\text{TEON}}})\|_{\text{TEON},*} \leq \sqrt{\frac{2L_{\text{TEON}}\Delta_0}{T}}. \quad (33)$$

From the NTR convergence guarantee under the $\|\cdot\|_{\text{MUON}}$ norm and the corresponding smoothness constant L_{MUON} , using the dual norm comparison in Lemma A.10, it follows that

$$\|\nabla f(\mathcal{W}_{\tau_{\text{MUON}}})\|_{\text{TEON},*} \leq \|\nabla f(\mathcal{W}_{\tau_{\text{MUON}}})\|_{\text{MUON},*} \leq \sqrt{\frac{2L_{\text{MUON}}\Delta_0}{T}}. \quad (34)$$

Using the smoothness-constant comparison in Lemma A.12, which states that $L_{\text{MUON}} \leq KL_{\text{TEON}}$, we have

$$\|\nabla f(\mathcal{W}_{\tau_{\text{MUON}}})\|_{\text{TEON},*} \leq \|\nabla f(\mathcal{W}_{\tau_{\text{MUON}}})\|_{\text{MUON},*} \leq \sqrt{K} \sqrt{\frac{2L_{\text{TEON}}\Delta_0}{T}}. \quad (35)$$

Under TEON norm metric, when the smoothness constant $L_{\text{TEON}} \approx L_{\text{MUON}}$, the convergence guarantees of TEON (the right hand side of Eq. (33)) and MUON (the right hand side of Eq. (34)) match up to constants.

In the best case, the convergence guarantees of TEON (the right hand side of Eq. (33)) and MUON (the right hand side of Eq. (35)) indicates that TEON has an improved convergence bound over MUON by up to a factor of \sqrt{K} .

which completes the proof. \square

A.6. Proof of Lemma 4.8

We prove the mode-1 case. The mode-2 case is symmetric.

Proof. Let $\mathcal{G} \in \mathbb{R}^{m \times n \times K}$ with slices $\mathbf{G}^{(k)} = \mathbf{u}^{(k)}\mathbf{v}^\top$, where $\mathbf{v} \in \mathbb{R}^n$ is shared across all k and $\{\mathbf{u}^{(k)}\}_{k=1}^K \subset \mathbb{R}^m$ are orthonormal. By definition of the MUON norm,

$$\|\mathcal{G}\|_{\text{MUON}} = \max_{1 \leq k \leq K} \|\mathbf{G}^{(k)}\|_{\text{op}} = \|\mathbf{v}\|_2.$$

The mode-1 matricization of \mathcal{G} satisfies

$$\mathcal{M}_1(\mathcal{G}) = [\mathbf{u}^{(1)}\mathbf{v}^\top \ \dots \ \mathbf{u}^{(K)}\mathbf{v}^\top] = \mathbf{U} \begin{bmatrix} \mathbf{v}^\top & & \\ & \ddots & \\ & & \mathbf{v}^\top \end{bmatrix},$$

where $\mathbf{U} = [\mathbf{u}^{(1)}, \dots, \mathbf{u}^{(K)}]$ has orthonormal columns. It follows that

$$\|\mathcal{G}\|_{\text{TEON}-1} = \|\mathcal{M}_1(\mathcal{G})\|_{\text{op}} = \sqrt{K} \|\mathbf{v}\|_2 = \sqrt{K} \|\mathcal{G}\|_{\text{MUON}}.$$

By definition, the smoothness constant associated with a norm $\|\cdot\|$ is

$$L_{\|\cdot\|} = \sup_{\|\Delta\| \leq 1} \|\nabla^2 f(\mathcal{W})[\Delta]\|_*.$$

Since the norm comparison $\|\Delta\|_{\text{TEON}-1} \leq \sqrt{K} \|\Delta\|_{\text{MUON}}$ is tight for tensors of the above form, the induced smoothness bound satisfies

$$L_{\text{MUON}} = K L_{\text{TEON}-1}.$$

\square

B. Pre-training Hyperparameters

B.1. Pre-training GPT

B.1.1. MODEL CONFIGURATION

Model	n_{embd}	n_{layer}	n_{head}	Param(M)
GPT-Small	768	12	12	124
GPT-Base	1024	24	16	362
GPT-Large	1280	36	20	774

Table 8. Architecture configurations of GPT models.

B.1.2. HYPERPARAMETERS FOR ADAMW ON GPT MODELS

Hyperparameter	GPT-Small	GPT-Base	GPT-Large
Learning rate	0.004	0.004	0.0001
Weight decay	0.1	0.1	0.1
LR scheduler	Cosine	Cosine	Linear
Warmup ratio	0.1	0.1	0.4

Table 9. Training hyperparameters for different model scales for AdamW. For the learning rate, we swept from 1e-4 to 6e-3, and the best setting is reported. For GPT-Large, we found that using the learning rate scheduler from (Amsel et al., 2025) yields the best performance. This schedule consists of a constant learning rate for the first 40% of training steps, followed by a linear decay to zero.

B.1.3. HYPERPARAMETERS FOR TEON/MUON ON GPT-SMALL

Hyperparameter	Muon	TEON
$Ortho(\cdot)$	Polar-Express	Polar-Express
Learning rate	0.005	0.005
LR scheduler	Cosine	Cosine
Weight decay	0.1	0.1
Warmup ratio	0.1	0.1
$Ortho(\cdot)$	You	You
Learning rate	0.005	0.005
LR scheduler	Cosine	Cosine
Weight decay	0.1	0.1
Warmup ratio	0.1	0.1
$Ortho(\cdot)$	Jordan	Jordan
Learning rate	0.005	0.005
LR scheduler	Cosine	Cosine
Weight decay	0.1	0.1
Warmup ratio	0.1	0.1

Table 10. Training hyperparameters for GPT-Small on FineWeb 10B tokens. We adopt the best learning rate reported in (Amsel et al., 2025). $K=2$ for all runs.

B.1.4. HYPERPARAMETERS FOR TEON/MUON ON GPT-BASE

Hyperparameter	MUON	TEON
<i>Ortho</i> (\cdot)	Polar-Express	Polar-Express
Learning rate	0.02	0.02
LR scheduler	Cosine	Cosine
Weight decay	0.1	0.1
Warmup ratio	0.1	0.1
<i>Ortho</i> (\cdot)	You	You
Learning rate	0.02	0.02
LR scheduler	Cosine	Cosine
Weight decay	0.1	0.1
Warmup ratio	0.1	0.1
<i>Ortho</i> (\cdot)	Jordan	Jordan
Learning rate	0.02	0.02
LR scheduler	Cosine	Cosine
Weight decay	0.1	0.1
Warmup ratio	0.1	0.1

Table 11. Training hyperparameters for GPT-Base on FineWeb 10B tokens. $K=2$ for all runs. We swept [0.005, 0.01, 0.02, 0.04] for the best learning rate.

B.1.5. HYPERPARAMETERS FOR TEON/MUON ON GPT-LARGE

Hyperparameter	MUON	TEON
<i>Ortho</i> (\cdot)	Polar-Express	Polar-Express
Learning rate	0.02	0.02
LR scheduler	Cosine	Cosine
Weight decay	0.1	0.1
Warmup ratio	0.1	0.1
<i>Ortho</i> (\cdot)	You	You
Learning rate	0.02	0.02
LR scheduler	Cosine	Cosine
Weight decay	0.1	0.1
Warmup ratio	0.1	0.1
<i>Ortho</i> (\cdot)	Jordan	Jordan
Learning rate	0.02	0.02
LR scheduler	Cosine	Cosine
Weight decay	0.1	0.1
Warmup ratio	0.1	0.1

Table 12. Training hyperparameters for GPT-Large on FineWeb 10B tokens. We adopt the best learning rate reported in (Amsel et al., 2025). $K=2$ for all runs.

B.2. Pre-training LLaMA

B.2.1. MODEL CONFIGURATION

Model	n_{embd}	n_{layer}	n_{head}	FFN dim	Param(M)
60M	512	8	8	1376	58
130M	768	12	12	2048	134
350M	1024	24	16	2736	368
1B	2048	24	32	5461	1339

Table 13. Architecture configurations of LLaMA-style models.

B.2.2. HYPERPARAMETERS FOR ADAMW

Hyperparameter	60M	130M	350M	1B
Learning rate	0.002	0.002	0.001	0.0001
Weight decay	0.1	0.1	0.1	0.1
LR scheduler	Cosine	Cosine	Cosine	Cosine
Warmup ratio	0.1	0.1	0.1	0.1

Table 14. Training hyperparameters for different model scales for AdamW. For the learning rate, we swept from 1e-4 to 4e-3, and the best setting is reported.

B.2.3. HYPERPARAMETERS FOR MUON

Hyperparameter	60M	130M	350M	1B
Learning rate	0.02	0.01	0.01	0.01
Weight decay	0.1	0.1	0.1	0.1
LR scheduler	Cosine	Cosine	Cosine	Cosine
Warmup ratio	0.1	0.1	0.1	0.1

Table 15. Training hyperparameters for different model scales for AdamW. For the learning rate, we swept [0.005, 0.01, 0.02], and the best setting is reported.

B.2.4. HYPERPARAMETERS FOR TEON

Hyperparameter	60M	130M	350M	1B
Learning rate	0.02	0.01	0.02	0.01
Weight decay	0.1	0.1	0.1	0.1
LR scheduler	Cosine	Cosine	Cosine	Cosine
Warmup ratio	0.1	0.1	0.1	0.1

Table 16. Training hyperparameters for different model scales for AdamW. For the learning rate, we swept [0.005, 0.01, 0.02], and the best setting is reported.

C. Additional Experiment Results

C.1. Alignment of top singular vectors

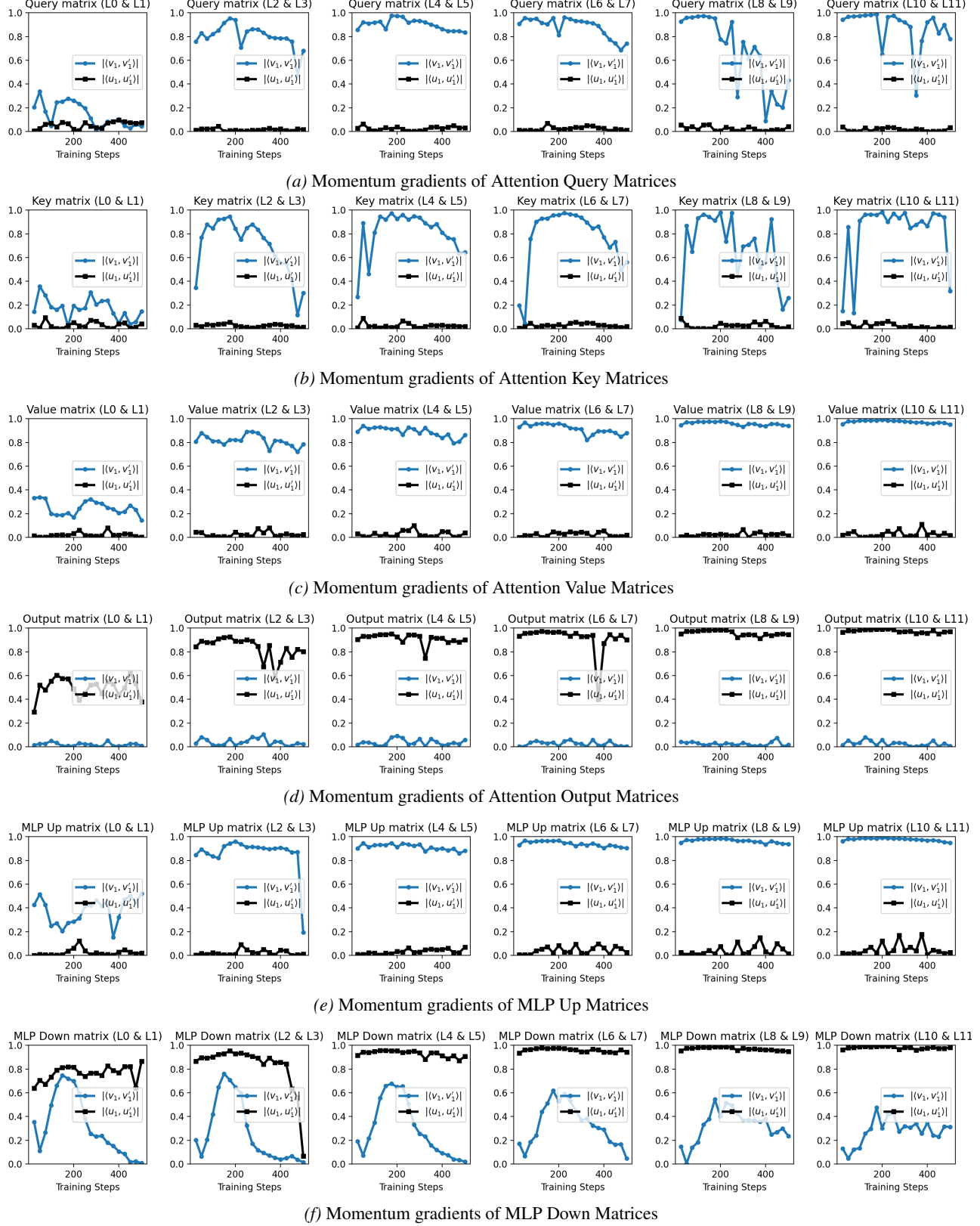


Figure 6. Inner product between top singular vectors of consecutive layer pairs.